Earth and Planetary Science Letters 479 (2017) 298–309

Contents lists available at ScienceDirect

Earth and Planetary Science Letters

www.elsevier.com/locate/epsl

An imbalance in the deep water cycle at subduction zones: The potential importance of the fore-arc mantle

Julia M. Ribeiro *, Cin-Ty A. Lee

Rice University, Earth Science Department, 77025 Houston, TX, USA

ARTICLE INFO

Article history:
Received 1 March 2017
Received in revised form 2 September 2017
Accepted 7 September 2017
Available online 5 October 2017
Editor: A. Yin

Keywords:
fore-arc mantle
subduction zones
water cycle
fluid dynamic
mass balance calculations
dragged-down serpentinites

ABSTRACT

The depth of slab dehydration is thought to be controlled by the thermal state of the downgoing slab: cold slabs are thought to mostly dehydrate beneath the arc front while warmer slabs should mostly dehydrate beneath the fore-arc. Cold subduction zone lavas are thus predicted to have interacted with greater extent of water-rich fluids released from the downgoing slab, and should thus display higher water content and be elevated in slab-fluid proxies (i.e., high Ba/Th, H_2O/Ce, Rb/Th, etc.) compared to hot subduction zone lavas. Arc lavas, however, display similar slab-fluid signatures regardless of the thermal state of the slab, suggesting more complexity to volatile cycling in subduction zones. Here, we explore whether the serpentinized fore-arc mantle may be an important fluid reservoir in subduction zones and whether it can contribute to arc magma generation by being dragged down with the slab. Using simple mass balance and fluid dynamics calculations, we show that the dragged-down fore-arc mantle could provide enough water (~7–78% of the total water injected at the trenches) to account for the water outfluxes released beneath the volcanic arc. Hence, we propose that the water captured by arc magmas may not all derive directly from the slab, but a significant component may be indirectly slab-derived via dehydration of dragged-down fore-arc serpentinites. Fore-arc serpentinite dehydration, if universal, could be a process that explains the similar geochemical fingerprint (i.e., in slab fluid proxies) of arc magmas.

1. Introduction

Subduction zones are one of the most important regions on Earth for volcanism, but the origin of such magmatism is unclear. The prevailing view is that arc magmatism is driven by hydrous flux melting by the passage of fluids released by prograde metamorphic dehydration reactions of the subducting slab (Grove et al., 2006; Kelley et al., 2010; Schmidt and Poli, 1998), but some recent studies suggest that arc magmatism might be largely driven by decompression in the convecting mantle wedge, with the effect of the slab fluids being secondary (England and Katz, 2010; Karlstrom et al., 2014; Turner and Langmuir, 2015a, 2015b). In the slab dehydration view, it is thought that the thermal evolution of the subducting slab, which controls dehydration, dictates where arc magmatism initiates. The depths at which dehydration takes place should thus depend on the initial thermal state of the slab (Peacock, 1990; Van Keken et al., 2011), which is primarily controlled by 1) the age of the plate, 2) the dip angle and 3) the rate of subduction (Syracuse et al., 2010). Indeed, cold and fast-sinking slabs, such as in the Marianas and Tonga, mostly dehydrate beneath the volcanic arc front, with remaining slab water contributing to back-arc magmatism or transported back into the deep mantle (Syracuse et al., 2010; Van Keken et al., 2011; Shaw et al., 2008) (Fig. 1A). However, the origin of arc magmas is likely to be more complicated. For example, for warm and young slab subduction, such as in Cascadia, thermal models predict that most of the intra-slab water is released well before the arc front (i.e., to serpentinize the cold fore-arc mantle) (Syracuse et al., 2010; Van Keken et al., 2011), suggesting that decompression melting may be the primary driver of arc magmatism.

Additional questions come from spatial and regional variations in arc water contents and various geochemical proxies for contributions from slab-derived fluids. For example, regardless of the type of subduction zone (cold or hot slab) and the location of the arc front in relation to when slab dehydration is predicted to occur, arc lavas display similar water contents (3.9 ± 0.45 wt%) (Plank et al., 2013; Walowski et al., 2015). Fluid-mobile versus fluid–immobile element ratios (H_2O/Ce, Rb/Th, Cs/Th, Ba/Th), which are thought to reflect fluid contributions from the slab, decrease in arc lavas with distance from the arc front (Fig. 2), as one might expect with progressive loss of water from the downgoing slab as it heats up (Plank et al., 2009; Van Keken et al., 2011). Yet, arc front lavas

* Corresponding author.
E-mail address: juliaribeiro@rice.edu (J.M. Ribeiro).

http://dx.doi.org/10.1016/j.epsl.2017.09.018
0012-821X/

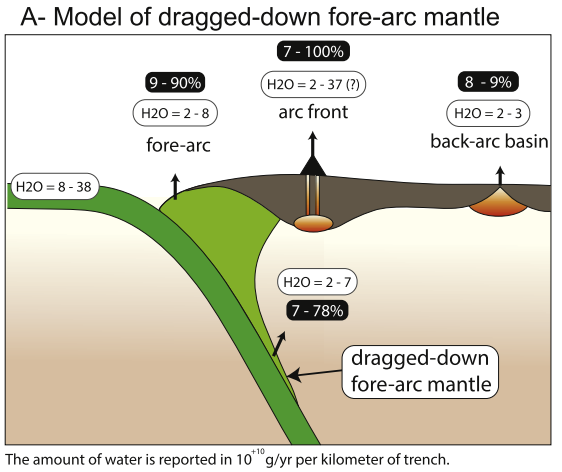

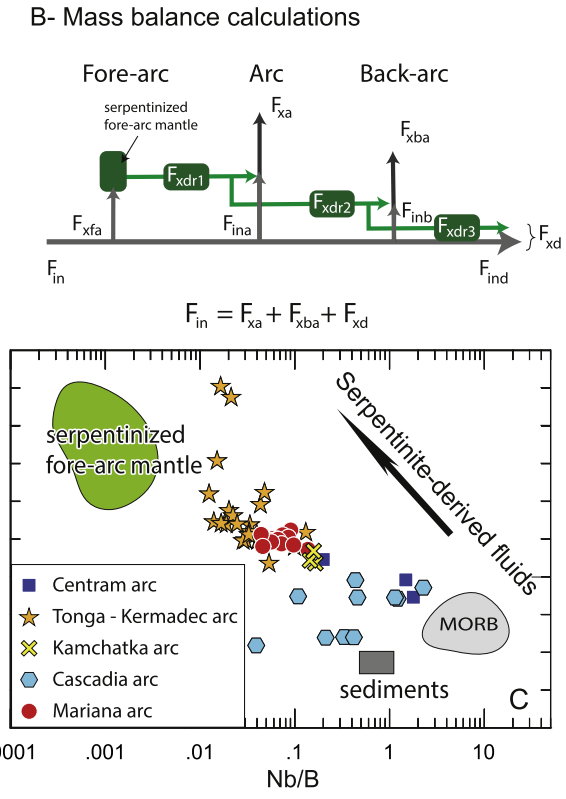

Fig. 1. Figures illustrating the potential role of the fore-arc mantle in the petrogenesis of arc magmas. A) Sketch showing the water budget of a typical subduction zone, with a dragged-down fore-arc mantle. The number represent the amount of water released from the downgoing plate for all the subduction zones investigated here (see Fig. 8 for details). The white numbers within a black oval represent the various water fluxes relative to the water influxes injected at the trenches (in %) as in Table 1 (i.e., for the fore-arc, F_{xfa}/F_{in}; for the arc, F_{xa}/F_{in}; for the back-arc, F_{xba}/F_{in}; for the water returned to the lower mantle F_{xd}/F_{in}). B) Sketch summarizing our mass balance calculations, as detailed in Eq. (1) and Eq. (5). Notations can be found in Table 2. C) Nb/B vs δ^{11}B diagram of Scambelluri and Tonarini (2012) used to decipher the contribution of the fore-arc serpentinites in arc lavas. Composition of the arc lavas are filtered for primitive composition (i.e., $SiO_2 \leq 56$ wt%, MgO $\geq$ 5 wt%) whenever possible. We used the dataset of Ishikawa and Tera (1999) for the Marianas, Leeman et al. (2004) for Cascadia, Ishikawa et al. (2001) for Kamchatka, Leeman et al. (2017) for Tonga–Kermadec, Tonarini et al. (2007) for Central America (Centram), and Marschall et al. (2017) for the mid-ocean ridge basalts (MORB) using an averaged Nb content of 6.3 ± 9.6 ppm (Jenner and O'Neill, 2012).

Table 1
Subduction parameters used in our modeling, and results of our mass balance calculation and 2D fluid dynamic modeling. We only report the results of our successful runs that are within the mass balance limitations imposed by Eq. (12).

		L (km)	u_0 (mm/yr)	α (°)	Age slab (Myr)	C_{H_2O} in arc (wt%)	M in arc (km²/Myr)	F_{xa} (g/yr/km)	C_{H_2O} in back-arc (wt%)	M in back-arc (km²/Myr)	F_{xba} (g/yr/km)	F_x (g/yr/km)	F_{xdr} (g/yr/km)	F_{in} (g/yr/km)	F_{xdr}/F_{in} (%)	F_{xa}/F_{in} (%)	F_{xba}/F_{in} (%)	Type of subduction zones
Mariana	min	1400	15	56.9	147.8			4.61E+10				6.70E+10	1.70E+10		7.01	19.03		cold
	max	1400	50	61.5	151.6	6.14	80.00	3.74E+11	2.78	268.00	2.09E+10	3.95E+11	5.58E+10	2.42E+11	23.00	154.15	8.60	
Tonga	min									261.30			3.45E+10					cold
	max	1350	170	52.1	165.8	3.91	80.00	2.77E+10	1.6	649.90	2.91E+10	5.69E+10	3.45E+10	3.84E+11	9.00	7.23 8.00	7.59	
Alaska–Aleutians	min	2700	49	42.0	47.1								1.71E+10		11.06			cold
	max	2700	64	55.9	56.1	6.46	80.00	1.83E+10				1.83E+10	3.09E+10	1.55E+11	20.00	11.87		
Cascadia	min	1300	30	19.8	10.0								1.07E+10		12.84			hot
	max	1300	40	22.4	6.9	3.59	80.00	5.59E+10				5.59E+10	6.48E+10	8.33E+10	77.79	67.08		
	Average		**60**	**44.37**	**83.61**	**5.03**	**80.00**	**1.04E+11**	**2.19**	**393.07**	**2.50E+10**	**1.19E+11**	**3.32E+10**	**2.16E+11**	**15.36**	**48.32**	**11.57**	
	1δ		*51*	*17.01*	*69.39*	*1.48*		*1.51E+11*	*0.83*	*222.45*	*5.84E+09*	*1.55E+11*	*1.91E+10*	*1.29E+11*				

Table 2
Notations.

ϕ slab thermal parameter	no units
F_{in} fluxes of water injected at the trenches	g/yr per kilometer of trench
F_{xd} fluxes of water returned to the lower mantle by the residual slab	g/yr per kilometer of trench
F_{xfa} fluxes of water released from the slab beneath the fore-arc mantle	g/yr per kilometer of trench
F_{x} fluxes of water released from the slab beneath the arc and the back-arc basin	g/yr per kilometer of trench
F_{xa} fluxes of water released from the slab beneath the arc	g/yr per kilometer of trench
F_{xba} fluxes of water released from the slab beneath the back-arc basin	g/yr per kilometer of trench
F_{xgas} fluxes of water released from the slab beneath the arc by volcanic degassing	g/yr per kilometer of trench
F_{xCO_2} fluxes of CO_2 released from the slab beneath the arc by volcanic degassing	g/yr per kilometer of trench
F_{ina} fluxes of slab-derived water released beneath the arc front	g/yr per kilometer of trench
F_{inb} fluxes of slab-derived water released beneath the back-arc basin	g/yr per kilometer of trench
F_{ind} fluxes of slab-derived water returned to the mantle	g/yr per kilometer of trench
F_{xdr} fluxes of water carried to depth by the dragged-down fore-arc serpentinites	g/yr per kilometer of trench
F_{xdr1} fluxes of dragged-down fore-arc water released beneath the arc front	g/yr per kilometer of trench
F_{xdr2} fluxes of dragged-down fore-arc water released beneath the back-arc	g/yr per kilometer of trench
F_{xdr3} fluxes of dragged-down fore-arc water returned to the lower mantle	g/yr per kilometer of trench
f_{xd} fraction of fore-arc mantle water that contributes to the water returned to the lower mantle	%
f_{xa} fraction of fore-arc mantle water that contributes to the water released beneath the arc	%
f_{xba} fraction of fore-arc mantle water that contributes to the water released beneath the back-arc basin	%
H thickness of the lithosphere	km
M magma addition or magma rate	km^2/Myr or km^3/Myr per kilometer of trench
ρ density	g/cm^3
C_{H_2O} water content	wt%
L trench length	km
D dilution factor	no units
TiO_2^{corr} PEC-corrected concentration in TiO_2 in the olivine-hosted melt inclusion	wt%
TiO_2^{meas} measured concentration in TiO_2 in the olivine-hosted melt inclusion	wt%
C_{corr} PEC-corrected concentration of the element of interest in the olivine-hosted melt inclusion	wt% or ppm
C_{meas} measured concentration of the element of interest in the olivine-hosted melt inclusion	wt% or ppm
τ shear stress	Pa
α subduction angle	degree
g mass acceleration due to gravity	9.81 m/s^2
$\Delta\rho$ difference in density between the serpentinite channel and the surrounding asthenospheric mantle. $\Delta\rho$ varies between 0.33 g/cm^3 for a mantle serpentinized at 50% and 0.65 g/cm^3 for a mantle serpentinized at 100% (Schwartz et al., 2001)	g/cm^3
h thickness of the serpentinite channel, and it can vary between 2 to 10 km thick (Hilairet et al., 2007; Schwartz et al., 2001)	km
y variable that varies between 0 and h	km
μ viscosity in the subduction channel can vary between 10^{+19} Pa·s and 10^{+20} Pa·s for a mantle serpentinized from 100% to 50%, respectively (Schwartz et al., 2001)	Pa·s
M_{dr} flux of dragged-down serpentinites	km^2/Myr
u velocity of the serpentinite fluid	mm/yr
u_0 convergence rate	mm/yr
Fo_{meas} forsterite content measured in olivine	no units
Fo_{eq} calculated forsterite content using melt inclusion composition	no units

from hot and cold subduction zones seem to display similar values of slab-fluid proxies in average ($H_2O/Ce_{arc} = 2267 \pm 1322$, $Rb/Th_{arc} = 14 \pm 10$, $Ba/Th_{arc} = 324 \pm 424$, $Cs/Th_{arc} = 0.63 \pm 1.00$ (1σ); Fig. 2), even though one might expect arc lavas in hot subduction zones to be less enriched in slab fluids due to earlier slab dehydration. The lack of correlation between the slab fluid proxies and the slab thermal parameter (Fig. 3) suggest that the model of water delivery to the mantle wedge by slab dehydration must be more complicated. Indeed, it has been suggested that the composition of primary arc magmas, except for the most fluid-mobile trace elements, is largely controlled by the thermal structure of the mantle wedge (i.e., the degree of mantle melting), with the slab flux playing a secondary role (Turner et al., 2016), making the similar water contents of arc magmas in hot and cold subductions even more perplexing.

Here, we explore the possibility that water delivery to the mantle wedge is not just controlled by release of fluids from the slab beneath the arc front. We evaluate the possibility that water is delivered to the mantle wedge by the serpentinized fore-arc mantle, in addition to direct dehydration of the slab, as originally proposed by Tatsumi (1989). To quantify the water outfluxes released at the arc and back-arc basin spreading center, we performed new mass balance calculations by using the maximum water content of olivine-hosted melt inclusions and basaltic glass shards, as well as gas outfluxes released at arc volcanoes. The extent to which the fore-arc mantle can be dragged down to subarc depths is assessed with simple fluid dynamic equations. We find that the downgoing plate does not carry enough water down to sustain the water outfluxes released in the Mariana and Cascadia arcs. We show that dragging down of fore-arc mantle, followed by its dehydration, is a viable mechanism that can compensate for this water imbalance.

2. The serpentinized fore-arc mantle: a potential source of water during subduction

There is growing evidence that cold fore-arc mantle is serpentinized by slab dehydration (<80–70 km depth), well before the arc front (Hyndman and Peacock, 2003). If this serpentinized fore-arc mantle could be dragged down by the subducting slab to subarc or back-arc depths, as hypothesized by some investigators (Hattori and Guillot, 2003; Horodyskyj et al., 2009; Scambelluri and Tonarini, 2012; Tatsumi, 1989), can its dehydration contribute to the water outflux in arcs, amplifying that derived directly from within the slab? Serpentinites have the capability to retain large amounts of water within their lattice (up to 13 wt%), and they can carry water down to 200 km depth through their transformation into chlorite and phase A (Komabayashi et al., 2004; Ulmer and Trommsdorff, 1995).

Whether the serpentinized fore-arc mantle is dragged-down or not with the downgoing plate is an open question. For instance, thermal modeling suggests that the cold and highly hy-

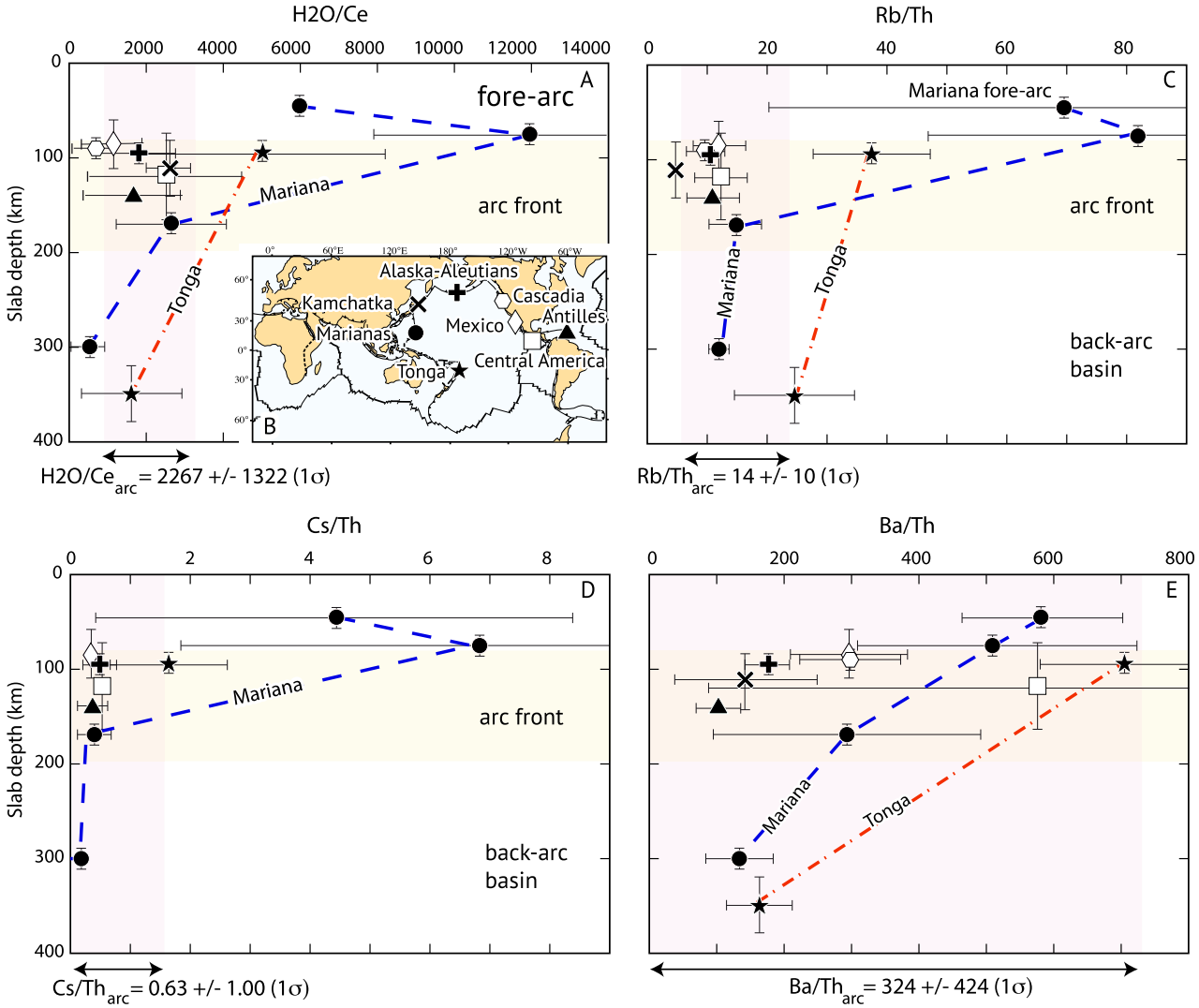

Fig. 2. Variations in the averaged slab-fluid proxies with increasing depths to the slab at cold (black symbols) and hot (white symbols) subduction zones. (A) Location map with the legend for our symbols. Arc lavas display similar averaged (B) H_2O/Ce, (C) Rb/Th and (D) Ba/Th ratios (Ribeiro et al., 2015) within errors (1σ) regardless of the type of the subduction zones. These averages in slab fluid proxies agree well with those calculated using the more comprehensive "raw" dataset of Turner and Langmuir (2015b) (i.e., $Rb/Th_{arc\_Turner} = 13.43 \pm 9.59$, $Cs/Th_{arc\_Turner} = 0.69 \pm 0.71$, $Ba/Th_{arc\_Turner} = 308.60 \pm 259.00$ (1σ); Fig. 3). The slab fluid proxies, however, clearly decrease with the increasing depth to the slab (i.e., from the arc to the back-arc basin), as shown here for the Marianas and Tonga and depicted by the blue and red dashed lines respectively. The dashed lines are simply connecting the dots for clarity. We use the dataset of Ribeiro et al. (2015) for consistency in the filtering and data processing (see section 5). (For interpretation of the colors in this figure, the reader is referred to the web version of this article.)

drous conditions observed in the fore-arc mantle are maintained if the fore-arc remains stagnant (and is not dragged-down) during subduction (Wada et al., 2008). Additionally, serpentinization decreases the density of peridotite (Reynard, 2013) so that such serpentinized mantle will tend to flow buoyantly back to the surface instead of being subducted (Hyndman and Peacock, 2003). However, exhumed fore-arc serpentinites at mountain belts are commonly associated with eclogites (Guillot et al., 2009, 2000; Hermann et al., 2000; Horodyskyj et al., 2009), which record pressures up to 2.7 GPa (~90 km depths), clearly demonstrating that serpentinites were either dragged down or formed at subarc depths (Erdman and Lee, 2014; Guillot et al., 2009; Schwartz et al., 2001). Geophysical studies have also shown the occurrence of a low-seismic velocity channel on top of the downgoing plate (Abers, 2000), which may represent a serpentinite channel. Enrichments in highly incompatible, fluid-mobile trace elements (Cs, Ba, Rb, As, B, etc.), $\delta^{11}B$ and elevated fluid signatures (Ba/Th > 800, Rb/Th > 100 for the fore-arc serpentinites) also hint at the presence of serpentinitized mantle as deep as beneath the arc (Fig. 1C) (Barnes et al., 2008; Hattori and Guillot, 2003; Savov et al., 2007; Scambelluri and Tonarini, 2012). For instance, 75% of the intra-slab boron is thought to be released during shallow slab dehydration beneath the fore-arc (Pabst et al., 2012; Savov et al., 2007), and the high boron content and associated $\delta^{11}B$ in arc lavas (Fig. 1C) is thus imparted to the dragged-down fore-arc mantle that dehydrates at subarc depth and further contributes to arc magmatism (Scambelluri and Tonarini, 2012; Straub and Layne, 2002). These observations can be interpreted to represent either down-dragged fore-arc serpentinites or serpentinization of the asthenospheric mantle in contact with the dehydrating slab.

For the following reasons, we suggest that serpentinized mantle inferred to occur beneath the arc could represent dragged down fore-arc material. Serpentinization significantly enhances the buoyancy of the fore-arc mantle, which should then express itself at the surface in the form of a fore-arc bulge due to isostatic effects (Fig. 4A). Yet, most fore-arcs are not characterized by a highly-pronounced topographic high (Gvirtzman and Stern, 2004; Wright et al., 2000). Furthermore, the serpentinized fore-arc wedge seems to have attained a steady state in terms of size, that is,

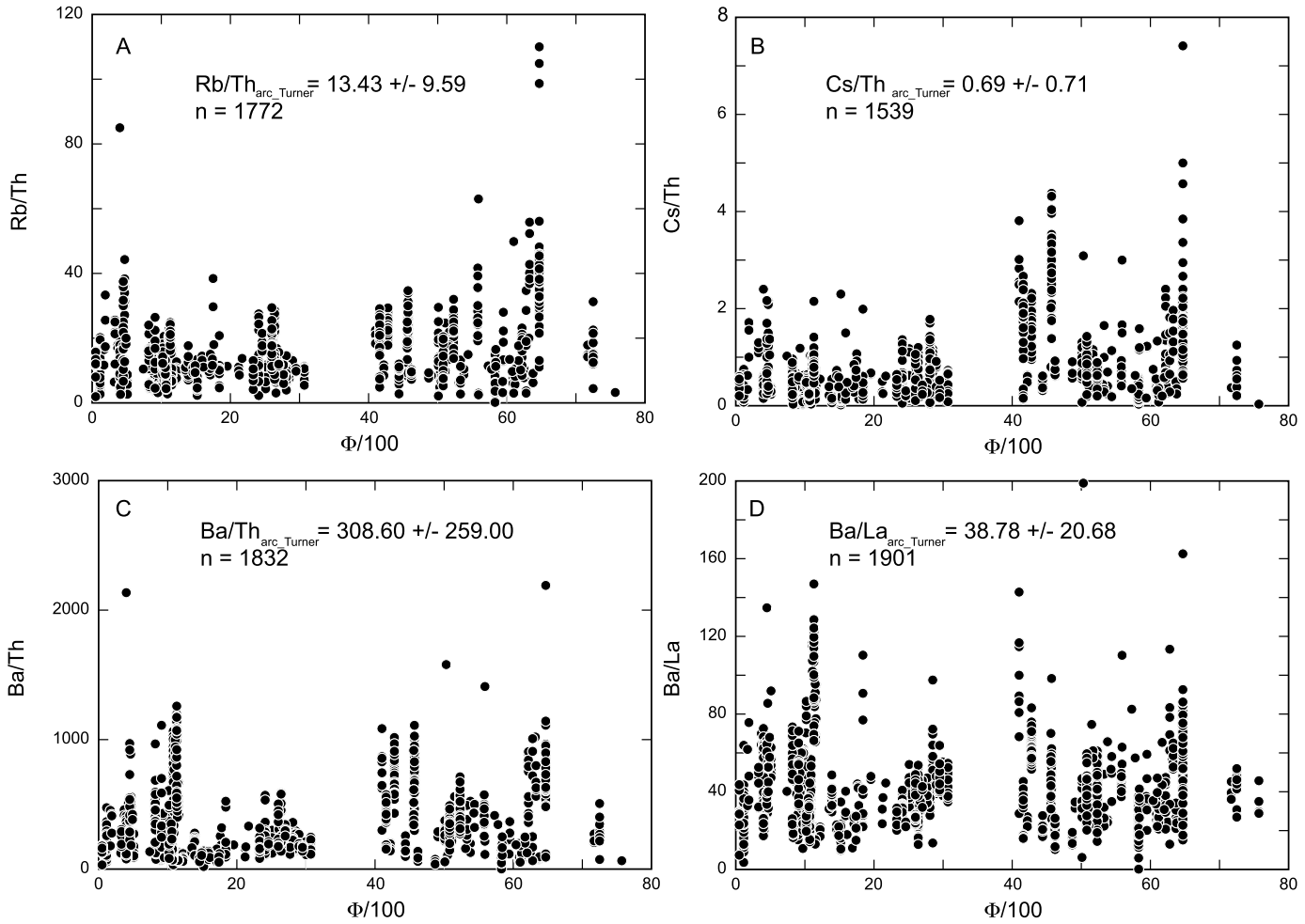

Fig. 3. Variations in the slab-fluid proxies with the slab thermal parameter ϕ for the worldwide arc volcanoes. We used the "raw" data compilation (entitled "GlobalArcsRawVals") of Turner and Langmuir (2015b). Lack of correlation between ϕ and the slab-fluid proxies (A) Rb/Th, (B) Cs/Th, (C) Ba/Th and (D) Ba/La suggest that the slab thermal parameter does not play a first-order role on the composition of arc magmas. Instead, hot slab (with a small ϕ) and cold slab (with a higher ϕ) magmas cannot be discriminated based upon their chemistry. Averages are reported with one standard deviation (1σ) to the mean, n is the number of samples averaged.

there is no evidence that the serpentinized fore-arc mantle grows in terms of size with time, even though the processes for making serpentinized wedge material continue. In fact, in a non-steady state fore-arc mantle, continuous serpentinization of the fore-arc mantle could cause the arc front to move away from the trench (Fig. 4A), which is not seen. In most cases, arc fronts are migrating towards the trench, as in the Marianas (Kato et al., 2003; Lallemand et al., 2005).

The steady state nature of the fore-arc mantle wedge and the lack of topographic highs suggests that serpentinized fore-arc mantle must be removed as fast as it is formed. One possibility is that the fore-arc mantle is dragged-down by the slab (Fig. 4B) (Tatsumi, 1989). The other possibility is that the serpentinized fore-arc mantle rises diapirically to the surface (Erdman and Lee, 2014) and erodes, but even so, the eroded material would accumulate in the trench and be subducted (Von Huene and Lallemand, 1990). Thus, in both scenarios, serpentinized fore-arc material is dragged back down into the mantle, either directly or indirectly. Stretching and faulting can also contribute to thinning and flattening of the fore-arc topography (Fryer et al., 1999; McCaffrey, 1992), although some fore-arcs are shortening (e.g., Mazzotti et al., 2002; McCaffrey et al., 2000). Stretching of the fore-arc will also promote upwellings of the buoyant serpentinites along normal faults (Farough et al., 2016; Savov et al., 2007), facilitating eruption of serpentinite mud volcanoes (Fryer, 1993; Fryer et al., 2006). Yet, most fore-arcs are not characterized by serpentinite eruption, implying that the continuous removal of the serpentinized fore-arc mantle might mostly occur at depth. We thus envision a steady state scenario in which the fore-arc mantle wedge is progressively replenished with new input of fresh asthenospheric mantle, which in turn becomes rapidly serpentinized as it interacts with the water-rich fluids released from the shallow part of the slab early in the subduction process. This serpentinized material is then returned back into the mantle by the downgoing slab (Savov et al., 2007; Tatsumi, 1989). Below, we quantitatively evaluate the plausibility of this scenario, originally hypothesized by Tatsumi (1989). If correct, the possibility that much of the water in arc lavas could be modulated by down-dragged fore-arc serpentinites will force us to re-examine the origin of arc magmas.

3. Estimating the water outfluxes using mass balance calculations

In this section, we evaluate water inputs and outputs into the subduction zone to test the plausibility of serpentinized fore-arc mantle in the origin of water in arc lavas. We assume steady state for these mass balance calculations, so that the amount of water injected at the trench associated with deserpentinization of the fore-arc mantle equals the total water outfluxes. Calculations were performed by considering that all the serpentinized fore-arc mantle is dragged down with the slab (i.e., $F_{xfa} = F_{xdr}$) as follows (Plank and Langmuir, 1998) (Fig. 1B):

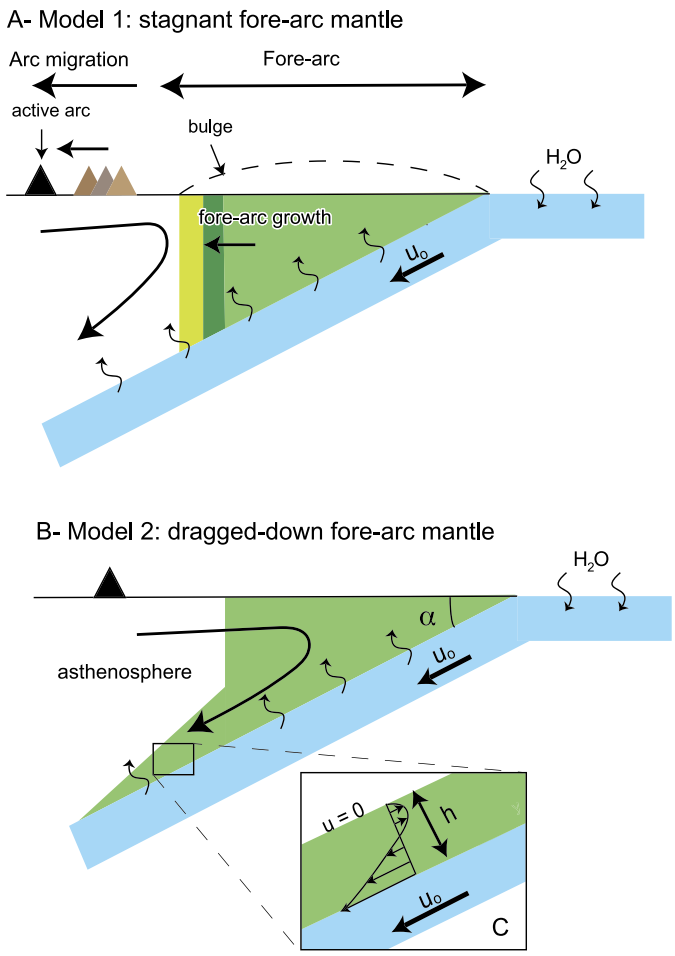

Fig. 4. Sketches showing a stagnant (A) vs. a dragged-down (B, C) serpentinized fore-arc mantle. A) In the case of a stagnant fore-arc mantle, the continuous serpentinization of the fore-arc mantle results in a bulge and the migration of the arc front away from the trench. B) The fore-arc mantle is dragged-down with the slab after being serpentinized during shallow slab dehydration. The serpentinite flow is driven by the pressure gradient applied along an inclined plane (i.e., the slab) and by the convergence rate (u_o). The no-slip boundary conditions imply that the asthenospheric mantle is a highly viscous material that convects very slowly compared to the low-viscosity dragged-down serpentinite flow (i.e., $u = 0$ at $h = y$). C) Sketch of the velocity profile of the serpentinite mantle flow in the subduction channel (see Fig. 5). α is the subduction angle.

$$F_{in} = F_{xa} + F_{xba} + F_{xd} \tag{1}$$

F_{in} is the total flux of water entering subduction zones, which is the sum of all components, such as pore water and mineral-bound water in sediments, oceanic crust and lithospheric mantle, that is, $F_{in} = u_0(\sum_i H^i C^i_{H_2O} \rho^i)$, where H is the thickness of the lithosphere (km), C_{H_2O} is the concentration of water and ρ is density. The right hand side of the equation is represented by all the output or exit fluxes: F_{xa} is the flux out of the arc front (g of water/yr/km of trench), F_{xba} is the outflux through the back-arc and F_{xd} is the outflux of remaining water that continues into the deep mantle. We define the flux of water from the slab into the fore-arc as F_{xfa}. This fore-arc water can then be dragged down into the mantle to contribute to magmatism or be recycled deep into the mantle. The fraction of fore-arc mantle that contributes to each of the exit fluxes in Eq. (1) is given by f_{xa}, f_{xba} and f_{xd}, such that

$$F_{xa} = f_{xa} F_{xfa} \tag{2}$$

$$F_{xba} = f_{xba} F_{xfa} \tag{3}$$

$$F_{xd} = (1 - f_{xa} - f_{xba}) F_{xfa} \tag{4}$$

We consider that the underlying serpentinized mantle in the slab has a constant thickness of 10 km and stores about 3.5 wt% water (this assumes that pure serpentinite has ~10 wt.% H_2O and the mantle is ~35% serpentinized) as in Emry et al. (2014). The water influxes and the subduction parameters (i.e., convergence rate u_o, subduction angle α) used in our modeling are from the literature (Plank and Langmuir, 1998), and detailed in Table 1 and in the supplementary materials. Steady state requires that water outfluxes released at the arc front and at the back-arc basin spreading center bound the amount of water released from the downgoing plate (Fig. 1B).

$$F_x = F_{xfa} + F_{xa} + F_{xba} \tag{5}$$

The flux of water transported to depth by the dragged-down fore-arc mantle (F_{xdr}), which contributes to magmatism or is recycled into the lower mantle, is (Fig. 1B):

$$F_{xdr} = \sum_i F^i_{xdr} \tag{6}$$

The fluxes of water out of the arc front and the back-arc basin or returned to the deep mantle thus integrate the water released from slab dehydration and from the dragged-down fore-arc serpentinites. These outfluxes are defined as follows,

$$F_{xa} = F_{xdr1} + F_{ina} \tag{7}$$

$$F_{xba} = F_{xdr2} + F_{inb} \tag{8}$$

$$F_{xd} = F_{xdr3} + F_{ind} \tag{9}$$

F_{ina}, F_{inb} and F_{ind} represent the fluxes of water released from the slab that are injected beneath the arc front and the back-arc basin or recycled into the mantle, respectively.

Water outfluxes released beneath the arc and back-arc basin spreading centers F_{xa} and F_{xba} (g/yr/km) were estimated using the water contents analyzed in olivine-hosted melt inclusions and glass shards. Melt inclusions, corrected for post-entrapment crystallization (see details in section 5), and glass shards were carefully scrutinized for minimally degassed, basaltic compositions ($SiO_2 \leq$ 56 wt%, MgO $\geq$ 5 wt%, $CO_2 <$ 50 ppm, S $<$ 500 ppm) (Kelley et al., 2010): 252 glass compositions from the Marianas, Alaska-Aleutian, Cascadia and Tonga convergent margins passed through this filter (details can be found in the supplementary Table S1). Because glasses have likely degassed water to some extent, we used the maximum water content from our filtered dataset to estimate the amount of water released at convergent margins. These maximum water contents likely represent minimum water estimates (Plank et al., 2013). Water outfluxes released beneath the arc and the back-arc basin spreading center can be expressed as the sum of the water trapped in glasses (as glass shards and olivine-hosted melt inclusions) and the water released by volcanic degassing F_{xgas}:

$$F_{xa} \text{ or } F_{xba} = \frac{M \rho C_{H_2O}}{L} + F_{xgas} \tag{10}$$

where ρ is the density of the crust (g/cm^3), C_{H_2O} is the primary water content in the melt inclusion and L is the trench length (km). The magma addition rate M (km^2/Myr) for the back-arc was estimated by multiplying the half spreading rate of the back-arc basin spreading center with its crustal thickness of 6.7 km. The magma addition rate for the arc was assumed to be 80 km^3/km/Myr as estimated from seismic crustal profiles (Calvert et al., 2008; Dimalanta et al., 2002; Holbrook et al., 1999) (see supplementary material and Table S2-1 for details). Because F_{xgas} has not been measured in back-arc basins yet, we only consider the water released by volcanic degassing beneath the arc front (i.e., $F_{xba} = \frac{M \rho C_{H_2O}}{L}$).

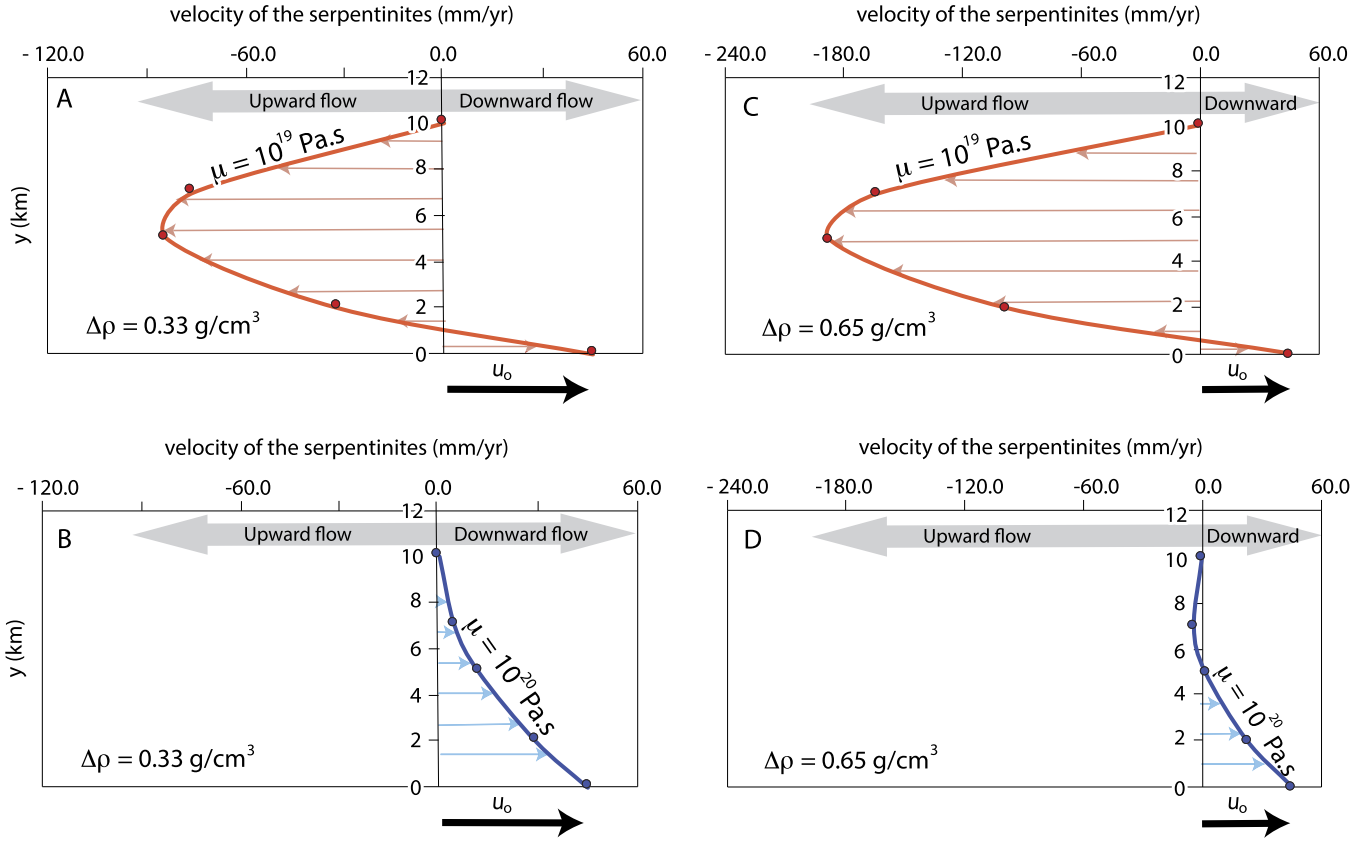

Fig. 5. Velocity profiles for the dragged-down fore-arc mantle (using Eq. (15)). The velocity profiles are modeled for a cold subduction zone, such as the Marianas (u_o = 47.5 mm/yr, $\alpha = 61.5°$) and the mantle is serpentinized at 50% ($\Delta\rho = 0.33$ g/cm^3) (A, B) and at 100% (C, D). When the viscosity μ of the serpentinite channel is 10^{+19} Pa·s (A, C), most of the serpentinites tend to flow back to the surface by buoyancy-driven flow. In contrast, when μ is 10^{+20} Pa·s (B, D), most of the serpentinites are dragged-down with the slab. Reasonable sizes of the serpentinite channel are 2 to 10 km thick (Hilairet et al., 2007); thus, here y varies between 0 to 10 km. See the method section for details about our calculations.

The water flux emitted at arc volcanoes by degassing F_{xgas} is assessed based upon the measured CO_2 fluxes, using a molar H_2O/CO_2 ratio of 50 (Hilton et al., 2002) for the Marianas (Supplementary Table S2-2). We also used the estimates of Fischer (2008) for the Aleutians, Kermadec and Central America arcs for the water fluxes released by volcanic degassing at the Alaska–Aleutians, Tonga and Cascadia arcs respectively. Our choice was guided by the closest location to our area of interest, as gas fluxes have not been measured everywhere yet.

4. Correction of the melt inclusion composition for post-entrapment crystallization

In this section, we outline how we estimate primary water contents in melt inclusions. Compositions of the olivine-hosted melt inclusions were first corrected for post-entrapment crystallization (PEC). Melt inclusions can crystallize olivine against their inclusion wall, resulting in an increase in Fe, volatiles and incompatible elements, and in a depletion in Mg in the melt inclusion composition (Kent, 2008). We can track back the composition of the melt inclusion prior to crystallization of olivine against the inclusion wall using simple calculations. We generally used the restored compositions of the melt inclusions that are reported by each study. However, when the composition of the melt inclusion is not corrected for post-entrapment processes, we performed the calculations by assuming $Fe^{3+}/\Sigma Fe = 0.25$ for the arc and 0.17 for the back-arc basin spreading center (Kelley and Cottrell, 2009), and using an exchange partition coefficient ($K_D^{\text{ol-liq}}$[Fe/Mg]) of 0.3 (Roeder and Emslie, 1970). Post-entrapment crystallization was corrected by adding olivine back in 0.1% increments to the measured composition until equilibrium with the olivine host is attained (i.e., $Fo_{meas} = Fo_{eq}$).

The volatile content of the melt inclusion was then restored by using a dilution factor as volatiles are also affected by post-entrapment processes:

$$D = \frac{TiO_2^{corr}}{TiO_2^{meas}} \tag{11}$$

$$C_{corr} = DC_{meas} \tag{12}$$

where D is the dilution factor, TiO_2^{meas} and TiO_2^{corr} are the concentrations in TiO_2 measured and corrected for post-entrapment crystallization respectively, and C_{corr} and C_{meas} are the PEC-corrected and measured concentrations of the element of interest, respectively. Here, we use the restored water content for our mass balance calculations.

5. Estimating the amount of water carried by the dragged-down serpentinites

In the following, we model the dragged-down fore-arc serpentinites as a 2D Newtonian viscous fluid (i.e., the velocity gradient of the fluid is proportional to the applied shear stress) along a subduction channel (Erdman and Lee, 2014; Gerya and Stöckhert, 2002; Schwartz et al., 2001). The viscosity μ of the fluid and the thickness h of the serpentinite channel (i.e., subduction channel composed of dragged-down serpentinites) are considered constant as we are only interested in first order behavior. The strain rate ($\frac{du}{dy}$) of a viscous Newtonian fluid scales with shear stress τ:

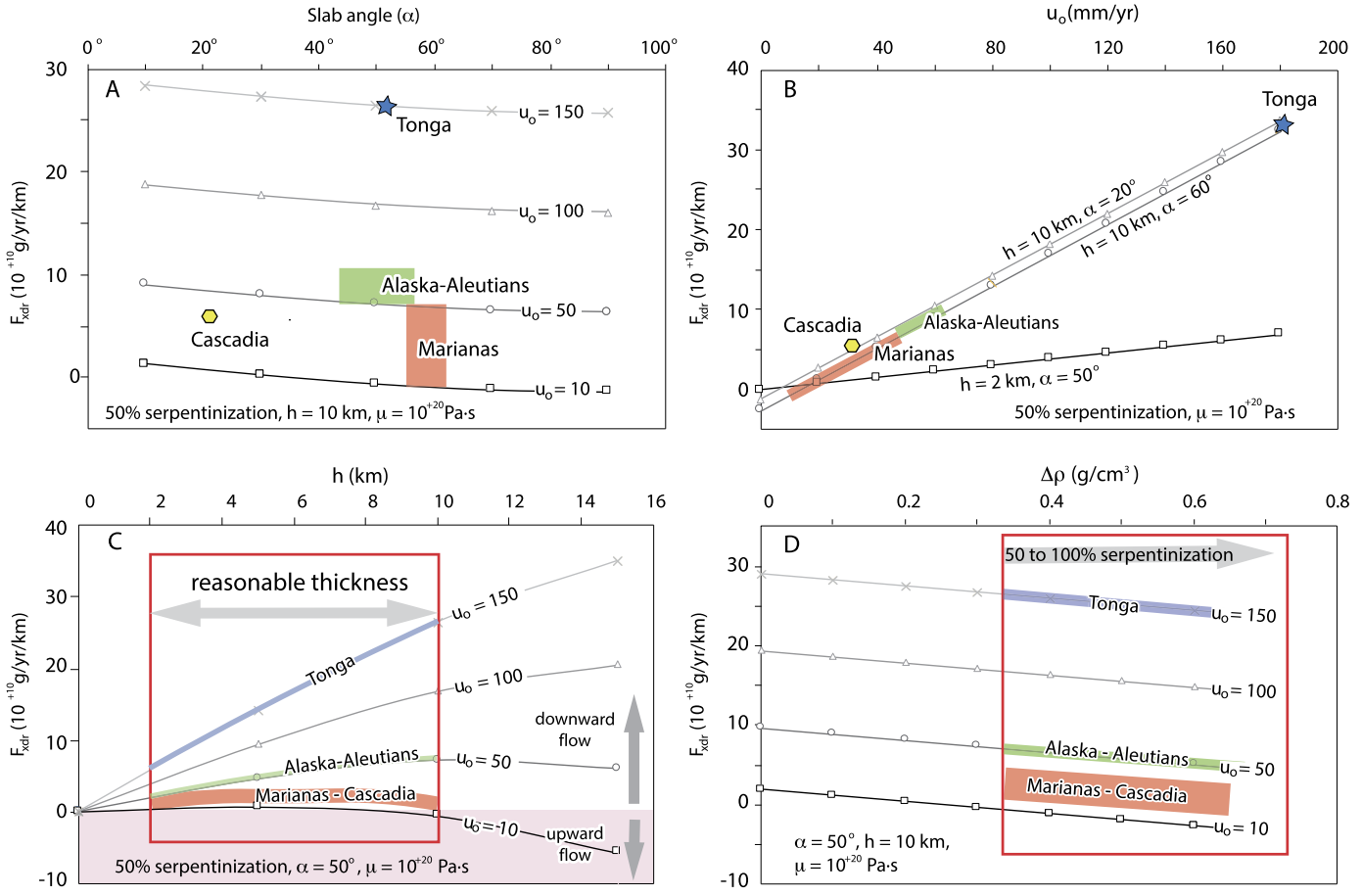

Fig. 6. Variations of the subduction parameters with the mass of water subducted by the serpentinite channel for a viscosity μ of 10^{+20} Pa·s (using Eq. (18)). A) the subduction angle α, B) plate velocity u_o (mm/yr), C) size of the subduction channel h and D) degree of serpentinization. (A, B) Fast and low-angle subduction zones will carry more serpentinite-bounded water to subarc depths. The amount of serpentinite-bounded water also increases with the thickness of the subduction channel (C) and decreases with the degree of serpentinization (D). The pink field in panel C depicts the region where the serpentinites flow back to the surface (upward flow); while the white field depicts the region where serpentinites are dragged downward. The fixed parameters in the different panels are 50% serpentinization (i.e., $\Delta\rho = 0.33$ g/cm^3), $h = 10$ km and $\alpha = 50°$. Details can be found in the method section and in Supplementary Table S2. (For interpretation of the references to color in this figure legend, the reader is referred to the web version of this article.)

$$\tau = \frac{du}{dy}\mu \tag{13}$$

where u is velocity, y is distance perpendicular to the direction of motion, and μ is viscosity (Pa·s). Force balance requires that the applied pressure gradient $\frac{dP}{dx}$ on the dragged-down serpentinites in the subduction channel equals the shear stress:

$$\frac{d\tau}{dy} = \frac{dP}{dx} \tag{14}$$

By combining Eq. (13) and Eq. (14) and integrating, we obtain an equation that describes the velocity of the serpentinite u in the subduction channel with a no-slip boundary condition (i.e., $u = 0$ at $y = h$) (Fig. 4C, 5):

$$u = \frac{1}{2\mu}\frac{dP}{dx}\left(y^2 - hy\right) - \frac{u_o y}{h} + u_o \tag{15}$$

where u_o is the plate velocity, x is the distance in the direction of motion and parallel to the plate, and h is the thickness of the channel. Eq. (15) implies that the velocity of the dragged-down serpentinite fluid is driven by the velocity of the slab u_o (Fig. 4C, 5) and the pressure gradient $\frac{dP}{dx}$, which is controlled by the buoyancy of the serpentinite channel:

$$\frac{dP}{dx} = \Delta\rho g \sin\alpha \tag{16}$$

where α is the dip angle, g is gravity, and $\Delta\rho$ is the intrinsic density contrast between serpentinite and peridotite, a quantity that we consider homogeneous throughout the subduction channel for simplification; but in reality it varies with depth depending upon the amount of water available from the slab as subduction proceeds. Because $\frac{dP}{dx} > 0$ and $\Delta\rho > 0$, the dragged-down fore-arc mantle will also tend to flow back to the surface by buoyancy-driven flow (Erdman and Lee, 2014; Gerya and Stöckhert, 2002; Hilairet et al., 2007; Schwartz et al., 2001) (Fig. 5A, C). Subduction parameters used in our modeling and water fluxes are summarized in Table 1; and details can be found in supplementary Table S2.

The mass of dragged-down serpentinites M_{dr} (km^2/yr) is obtained by integrating Eq. (8):

$$M_{dr} = \int_0^h u dy \tag{17}$$

$$M_{dr} = \frac{1}{2\mu}\frac{dP}{dx}\left(-\frac{h^3}{6}\right) + \frac{h\,u_o}{2} \tag{18}$$

The water flux transported to depth by the dragged-down serpentinites F_{xdr} (g/yr/km) is then inferred using the equation $F_{xdr} = \frac{M_{dr}\rho C_{H_2O}}{L}$. In our model, we allow serpentinization extent to vary between 50% and 100% (Supplementary Table S2), as inferred from seismic and petrographic observations of the fore-arc man-

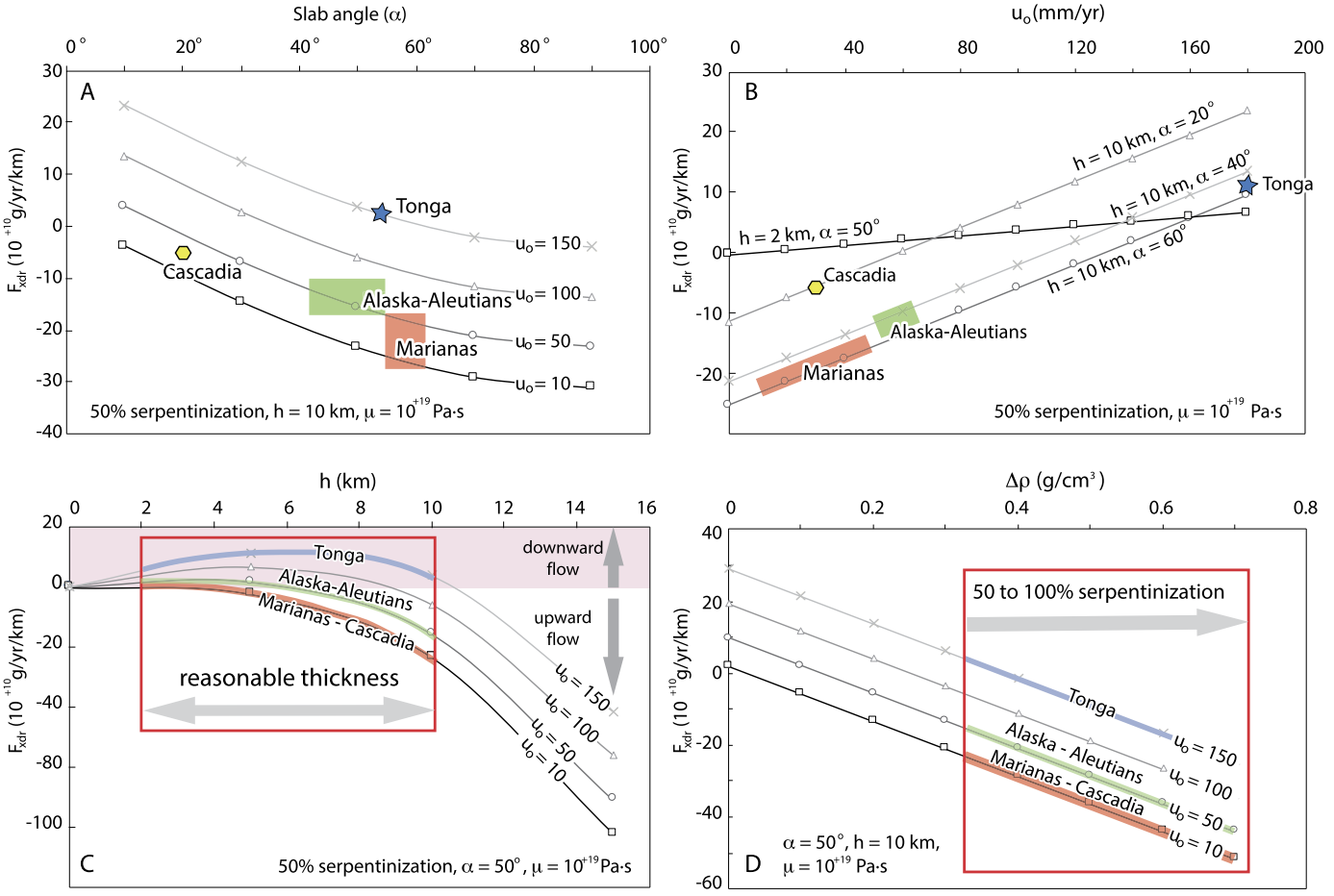

Fig. 7. Variations of the subduction angle α (A), channel thickness h (B), plate velocity u_o (C), and degree of serpentinization (D) with the mass of water transported by the serpentinite channel for a viscosity μ of 10^{+19} Pa·s (using Eq. (18)). Compared to Fig. 6 (where $\mu = 10^{+20}$ Pa·s), we note that most of the dragged-down serpentinites flow back to the surface by buoyancy-driven flow. We used 50% serpentinization (i.e., $\Delta\rho = 0.33$ g/cm^3), $h = 10$ km and $\alpha = 50°$ for our modeling. The pink field in panel C depicts the region where the serpentinites are dragged downward; while the white field depicts the region where serpentinites flow back to the surface (upward flow). Details can be found in Supplementary Table S2. Convergence rates u_o are reported in mm/yr. (For interpretation of the references to color in this figure legend, the reader is referred to the web version of this article.)

tle (Barklage et al., 2015; Hyndman and Peacock, 2003; Savov et al., 2007). However, because serpentinized ultramafic rocks were recovered in the fore-arc (Michibayashi et al., 2009; Ohara et al., 2008, 2012; Parkinson and Pearce, 1998), 50% to 80% serpentinization of the fore-arc mantle is a more realistic approximation.

Mass conservation requires that the downward flux of water associated with dragged-down serpentinites F_{xdr} not exceed the rate of serpentinization of the fore-arc mantle wedge, that is,

$$F_{xdr} \leq F_{xfa} \tag{19}$$

Our 2D fluid dynamic modeling (Eq. (18)) shows that the mass of water transported to depths by the dragged-down fore-arc mantle is primarily controlled by the viscosity of the serpentinite channel and the convergence rate, as depicted in Fig. 5A, B. For instance, if serpentine has a viscosity of 10^{+20} Pa·s (Hilairet et al., 2007; Schwartz et al., 2001), most of the serpentinites will be dragged-down with the slab (Fig. 5B, 6). In contrast, if the serpentinite channel has a viscosity of 10^{+19} Pa·s (Fig. 5B, 7), most of the serpentinites will flow back to the surface by buoyancy-driven flow (i.e., towards negative values in Fig. 5A, B). It is important to note that even if the fore-arc mantle is fully serpentinized, it can be dragged-down with the slab (and carries water to subarc depths) if the viscosity is 10^{+20} Pa·s (Fig. 5, 6). The degree of serpentinization of the serpentinite channel (modeled with varying $\Delta\rho$ in Fig. 6D, 7D), the thickness of the serpentinite channel h and the geometry of the fore-arc mantle (modeled with varying subduction angle α in Fig. 6B, 7B) thus produce second-order effects on the mass of water transported to depth by the dragged-down serpentinites.

6. An imbalance in the deep water cycle: importance of the dragged-down fore-arc mantle?

Our new mass balance calculations suggest that an imbalance in water exists for the Mariana and Cascadia convergent margins, and the slab does not carry enough water to explain the water outfluxes estimated beneath the arc. Indeed, intra-slab water may not bypass the Mariana arc front (42% to more than 100% slab water is lost beneath the fore-arc and the arc front); and the residual slab cannot sustain for the water outfluxes observed in the back-arc basin (Fig. 8A). As for the Cascadia arc (Fig. 8D), slab thermal models suggest that the Pacific plate has dehydrated by 90% to serpentinize the fore-arc mantle (Van Keken et al., 2011). If this prediction is correct, then the residual slab does not carry enough water downward to account for the water fluxes released beneath the Cascadia arc (i.e., we estimate that ~70% of intra-slab water is required for arc magmatism; Fig. 8D). Our results further imply that 1) slab influxes might be underestimated for the Mariana and Cascadia convergent margins, or 2) dehydration of the dragged-down fore-arc serpentinite contributes to arc (and perhaps back-arc) magmatism. Despite that slab influxes are poorly known,

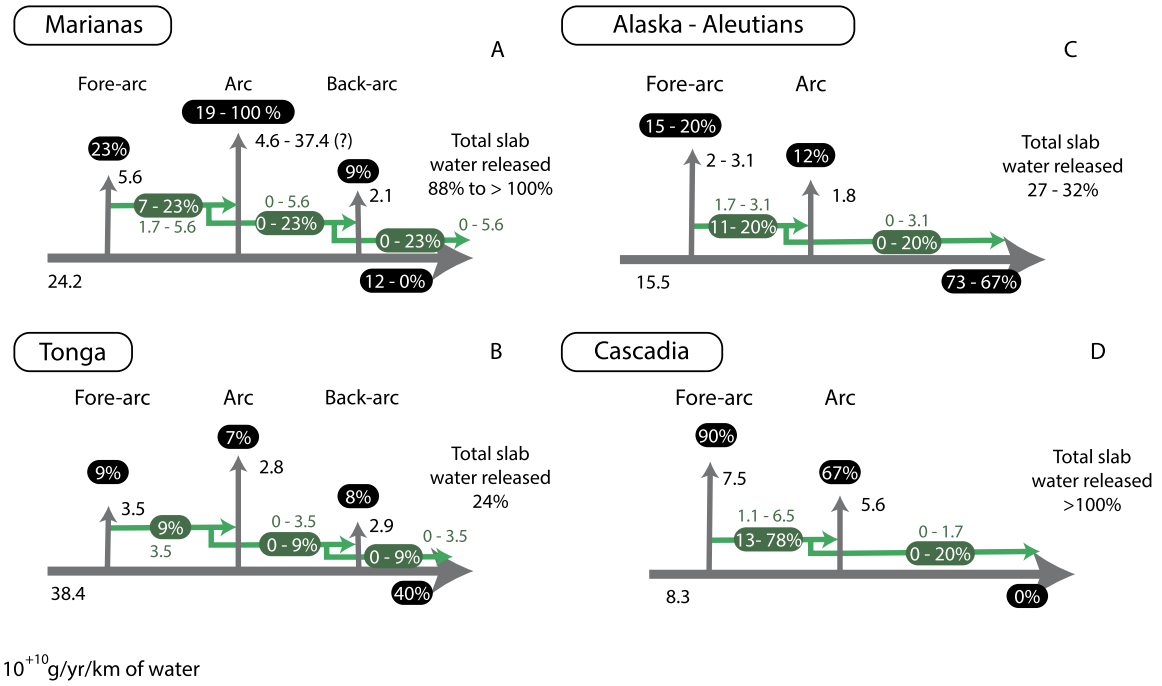

Fig. 8. Sketch summarizing our estimated water fluxes for the Mariana (A), Tonga (B), Alaska–Aleutian (C) and Cascadia (D) convergent margins. Black numbers represent water flux estimates in 10^{+10} g/yr per kilometer of trench, and white numbers within black ovals represent the water fluxes (in %) released beneath the arc (i.e., F_{xa}/F_{in}), the back-arc basin (i.e., F_{xba}/F_{in}) and returned to the lower mantle relatively to the water influxes injected at the trenches (i.e., F_{ind}/F_{in}). The white numbers within the green ovals are the water outfluxes (in %) released from the dragged-down fore-arc mantle relatively to the slab influxes (i.e., F_{xdr}/F_{in}), as in Fig. 1B. The grey arrows (and associated numbers) represent water fluxes estimated by mass balance calculations; while the green arrows (and associated green numbers) are the water fluxes carried by the dragged-down serpentinites F_{xdr} estimated using Eq. (18). The total water fluxes released from slab dehydration solely (in %) are estimated using Eq. (1), and they do not include the water fluxes released from the dragged-down fore-arc mantle (i.e., $F_{xdr} = 0$ in Eq. (7)–(9)). See text for details. (For interpretation of the references to color in this figure, the reader is referred to the web version of this article.)

our mass balance calculations use the most recent estimates of the amount of water input at the trenches (see Table S1 for details). Even if a greater amount of water is entering at the Cascadia trench, the slab is thought to mostly dehydrate beneath the fore-arc (Van Keken et al., 2011), so that an additional source of water to the slab is required to sustain water contents of arc magmas in hot subduction zones. Finally, we need to reconcile the observations that the slab-fluid proxies display similar averaged values in hot and cold subduction zone arc lavas (Fig. 2); and these proxies are not correlated with the slab thermal parameter ϕ (Fig. 3). For these reasons, we have explored here the possibility of the fore-arc mantle being dragged down with the subducting plate.

Our 2D fluid dynamic model suggests that the dragged-down fore-arc mantle can provide enough water to account for the water imbalance observed in the Mariana and Cascadia arcs (Fig. 8A, D). Although not necessary, the dragged-down fore-arc mantle can provide an additional source of water for the Alaska–Aleutians and Tonga convergent margins (Fig. 8B, C). Water can be carried by the fore-arc mantle within a 2 to 10-km thick channel, serpentinized to 50 to 100%, with a viscosity of 10^{+20} Pa·s (Fig. 5A–B and 6). Our model further shows that the dragged-down fore-arc mantle can transport up to $5.6 \times 10^{+10}$ g/yr/km (~23% of intra-slab water) of water beneath the arc front of cold subduction zones (i.e., Marianas, Tonga, Alaska–Aleutians; Fig. 8A–C). This contribution is more important for the Cascadia arc, where the dragged-down fore-arc mantle can transport up to $6.5 \times 10^{+10}$ g/yr/km of serpentinite-bounded water (~78% intra-slab water; Fig. 8D).

On average, the dragged-down fore-arc mantle can carry ~$3.1 \times 10^{+10}$ g/yr/km of water downward (~15% of averaged intra-slab water). The minimum of serpentinite-bounded water is transported to depth with the Mariana fore-arc mantle ($1.1 \times 10^{+10}$ g/yr/km; Table 1); while the maximum serpentinite-water flux is observed for the Cascadia fore-arc mantle ($6.5 \times 10^{+10}$ g/yr/km). This is a consequence of the mass balance limitations set by Eq. (19). Without any such limitations, the Cascadia fore-arc mantle delivers the minimum water flux into the subarc mantle (~$1.1 \times 10^{+10}$ to $6.5 \times 10^{+10}$ g/yr/km), while the Tonga fore-arc mantle can release up to $30 \times 10^{+10}$ g/yr/km of serpentinite-bounder water. This result mainly reflects the importance of the convergence rate on the flux of fore-arc serpentinites dragged down to depth (Fig. 6, 7).

7. Conclusions and future directions

Our new mass balance calculations coupled with simple fluid dynamic equations suggest a potential role of the serpentinized fore-arc mantle in the deep volatile cycle. An additional source of water to the slab is essential to account for the water outfluxes released beneath the Mariana and Cascadia arcs. The dragged-down fore-arc mantle can provide enough water to compensate for this water imbalance. We thus show that the fore-arc mantle is a temporary sink for water, but if it gets dragged down into the mantle, it can become an additional source for water (and other volatiles) that can contribute to the arc and back-arc magmatism. If the dragged-down fore-arc serpentinites contribute to the arc water budget, the residual slab can carry enough intra-slab water to dehydrate beneath the back-arc basin spreading center and recycle water in the lower mantle. In addition, this simple mechanism could explain why arc lavas display similar averaged water content and similar ratios in slab fluid proxies in hot and cold subduction zones.

Our study emphasizes the need to better constrain and quantify the contribution of the dragged-down fore-arc mantle in the generation of arc magmas and in the deep volatile cycle. We recognize that our hypothesis is speculative and there are undoubtedly many uncertainties and factors that still need to be consid-

ered. For example, we have not modeled the efficiency by which dragged down fore-arc serpentinites dehydrate. In addition, the ability for fore-arc serpentinites to be dragged down, as noted above, depends significantly on the rheology of the serpentinite. There is also the issue of how representative water contents in melt inclusions are of the actual flux of water through arc magmas. Future avenues of research could include 1) more sophisticated fluid dynamic modeling, which includes thermal evolution, metamorphism, and better rheological constraints; 2) slab dehydration experiments at shallow slab depths (i.e., beneath the fore-arc); 3) better quantification of slab water influxes injected at the trenches and water outfluxes released beneath the fore-arc mantle; and 4) development of new chemical proxies that discriminate slab fluids from the fluids released from the dragged-down fore-arc mantle. Additional ways of testing our hypothesis might be to extend our approach to estimating inputs and outputs of fluid mobile elements as possible proxies for water or serpentinized fore-arc mantle.

Acknowledgements

We would like to thank M. Farner and C. Fliedner (Rice University) for their help with the fluid dynamic equations, and M. Erdman (Rice University) for her comments on the exhumation processes. Discussions with T. Plank (LDEO) and T. Fischer (University of New Mexico) during the CIDER 2015 workshop, and J. Gill (UCSC), A. Kent (Oregon State University), C. Macpherson (Durham University), the editor An Yin for handling our manuscript and two anonymous reviewers greatly benefited this research project. This work was partially supported by an NSF grant (EAR-1347085) to Lee.

Appendix A. Supplementary material

Supplementary material related to this article can be found online at https://doi.org/10.1016/j.epsl.2017.09.018.

References

Abers, G.A., 2000. Hydrated subducted crust at 100–250 km depth. Earth Planet. Sci. Lett. 176, 323–330.

Barklage, M., Wiens, D.A., Conder, J.A., Pozgay, S.H., Shiobara, H., Sugioka, H., 2015. P and S velocity tomography of the Mariana subduction system from a combined land-sea seismic deployment. Geochem. Geophys. Geosyst. 16, 681–704.

Barnes, J.D., Sharp, Z.D., Fischer, T.P., 2008. Chlorine isotope variations across the Izu–Bonin–Mariana arc. Geology 36, 883–886.

Calvert, A.J., Klemperer, S.L., Takahashi, N., Kerr, B.C., 2008. Three-dimensional crustal structure of the Mariana island arc from seismic tomography. J. Geophys. Res., Solid Earth 113, B01406. http://dx.doi.org/10.1029/2007JB004939.

Dimalanta, C., Taira, A., Yumul Jr, G.P., Tokuyama, H., Mochizuki, K., 2002. New rates of western Pacific island arc magmatism from seismic and gravity data. Earth Planet. Sci. Lett. 202, 105–115.

Emry, E.L., Wiens, D.A., Garcia-Castellanos, D., 2014. Faulting within the Pacific plate at the Mariana Trench: implications for plate interface coupling and subduction of hydrous minerals. J. Geophys. Res., Solid Earth 119, 2013JB010718.

England, P.C., Katz, R.F., 2010. Melting above the anhydrous solidus controls the location of volcanic arcs. Nature 467, 700–703.

Erdman, M.E., Lee, C.-T.A., 2014. Oceanic- and continental-type metamorphic terranes: occurrence and exhumation mechanisms. Earth-Sci. Rev. 139, 33–46.

Farough, A., Moore, D.E., Lockner, D.A., Lowell, R.P., 2016. Evolution of fracture permeability of ultramafic rocks undergoing serpentinization at hydrothermal conditions: an experimental study. Geochem. Geophys. Geosyst. 17, 44–55.

Fischer, T.P., 2008. Fluxes of volatiles (H_2O, CO_2, N_2, Cl, F) from arc volcanoes. Geochem. J. 42, 21–38.

Fryer, P., 1993. The relationship between tectonic deformation, volcanism, and fluid venting in the southeastern Mariana convergent plate margin. In: Proceedings of JAMSTEC Symposium on Deep Sea Research, pp. 161–179.

Fryer, P., Gharib, J., Ross, K., Savov, I., Mottl, M.J., 2006. Variability in serpentinite mudflow mechanisms and sources: ODP drilling results on Mariana fore-arc seamounts. Geochem. Geophys. Geosyst. 7, Q08014. http://dx.doi.org/10.1029/2005gc001201.

Fryer, P., Wheat, C.G., Mottl, M.J., 1999. Mariana blueschist mud volcanism: implications for conditions within the subduction zone. Geology 27, 103–106.

Gerya, T.V., Stöckhert, B., 2002. Exhumation rates of high pressure metamorphic rocks in subduction channels: the effect of rheology. Geophys. Res. Lett. 29, 102-101–102-104.

Grove, T.L., Chatterjee, N., Parman, S.W., Médard, E., 2006. The influence of H_2O on mantle wedge melting. Earth Planet. Sci. Lett. 249, 74–89.

Guillot, S., Hattori, K., Agard, P., Schwartz, S., Vidal, O., 2009. Exhumation processes in oceanic and continental subduction contexts: a review. In: Lallemand, S., Funiciello, F. (Eds.), Subduction Zone Geodynamics. Springer, Berlin, Heidelberg, pp. 175–205.

Guillot, S., Hattori, K.H., de Sigoyer, J., 2000. Mantle wedge serpentinization and exhumation of eclogites: insights from eastern Ladakh, northwest Himalaya. Geology 28, 199–202.

Gvirtzman, Z., Stern, R.J., 2004. Bathymetry of Mariana trench-arc system and formation of the Challenger Deep as a consequence of weak plate coupling. Tectonics 23, TC2011. http://dx.doi.org/10.1029/2003tc001581.

Hattori, K.H., Guillot, S., 2003. Volcanic fronts form as a consequence of serpentinite dehydration in the fore-arc mantle wedge. Geology 31, 525–528.

Hermann, J., Müntener, O., Scambelluri, M., 2000. The importance of serpentinite mylonites for subduction and exhumation of oceanic crust. Tectonophysics 327, 225–238.

Hilairet, N., Reynard, B., Wang, Y., Daniel, I., Merkel, S., Nishiyama, N., Petitgirard, S., 2007. High-pressure creep of serpentine, interseismic deformation, and initiation of subduction. Science 318, 1910–1913.

Hilton, D.R., Fischer, T.P., Marty, B., 2002. Noble gases and volatile recycling at subduction zones. Rev. Mineral. Geochem. 47, 319–370.

Holbrook, W.S., Lizarralde, D., McGeary, S., Bangs, N., Diebold, J., 1999. Structure and composition of the Aleutian island arc and implications for continental crustal growth. Geology 27, 31–34.

Horodyskyj, U., Lee, C.T.A., Luffi, P., 2009. Geochemical evidence for exhumation of eclogite via serpentinite channels in ocean–continent subduction zones. Geosphere 5, 426–438.

Hyndman, R.D., Peacock, S.M., 2003. Serpentinization of the fore-arc mantle. Earth Planet. Sci. Lett. 212, 417–432.

Ishikawa, T., Tera, F., 1999. Two isotopically distinct fluid components involved in the Mariana arc: evidence from Nb/B ratios and B, Sr, Nd, and Pb isotope systematics. Geology 27, 83–86.

Ishikawa, T., Tera, F., Nakazawa, T., 2001. Boron isotope and trace element systematics of the three volcanic zones in the Kamchatka arc. Geochim. Cosmochim. Acta 65, 4523–4537.

Jenner, F.E., O'Neill, H.S.C., 2012. Analysis of 60 elements in 616 ocean floor basaltic glasses. Geochem. Geophys. Geosyst. 13, Q02005. http://dx.doi.org/10.1029/2011gc004009.

Karlstrom, L., Lee, C.T.A., Manga, M., 2014. The role of magmatically driven lithospheric thickening on arc front migration. Geochem. Geophys. Geosyst. 15, 2655–2675.

Kato, T., Beavan, J., Matsushima, T., Kotake, Y., Camacho, J.T., Nakao, S., 2003. Geodetic evidence of back arc spreading in the Mariana Trough. Geophys. Res. Lett. 30, 1625. http://dx.doi.org/10.1029/2002GL016757.

Kelley, K.A., Cottrell, E., 2009. Water and the oxidation state of subduction zone magmas. Science 325, 605–607.

Kelley, K.A., Plank, T., Newman, S., Stolper, E.M., Grove, T.L., Parman, S.W., Hauri, E.H., 2010. Mantle melting as a function of water content beneath the Mariana arc. J. Petrol. 51, 1711–1738.

Kent, A.J.R., 2008. Melt inclusions in basaltic and related volcanic rocks. Rev. Mineral. Geochem. 69, 273–331.

Komabayashi, T., Omori, S., Maruyama, S., 2004. Petrogenetic grid in the system $MgO–SiO_2–H_2O$ up to 30 GPa, 1600 °C: applications to hydrous peridotite subducting into the Earth's deep interior. J. Geophys. Res., Solid Earth 109, B03206.

Lallemand, S., Heuret, A., Boutelier, D., 2005. On the relationship between slab dip, back-arc stress, upper plate absolute motion, and crustal nature in subduction zones. Geochem. Geophys. Geosyst. 6, 1–18.

Leeman, W.P., Tonarini, S., Chan, L.H., Borg, L.E., 2004. Boron and lithium isotopic variations in a hot subduction zone—the southern Washington Cascades. Chem. Geol. 212, 101–124.

Leeman, W.P., Tonarini, S., Turner, S., 2017. Boron isotope variations in Tonga–Kermadec–New Zealand arc lavas: implications for the origin of subduction components and mantle influences. Geochem. Geophys. Geosyst. 18, 1126–1162.

Marschall, H.R., Wanless, V.D., Shimizu, N., von Strandmann P. A. E, Pogge, Elliott, T., Monteleone, B.D., 2017. The boron and lithium isotopic composition of mid-ocean ridge basalts and the mantle. Geochim. Cosmochim. Acta 207, 102–138.

Mazzotti, S., Dragert, H., Hyndman, R.D., Miller, M.M., Henton, J.A., 2002. GPS deformation in a region of high crustal seismicity: N. Cascadia fore-arc. Earth Planet. Sci. Lett. 198, 41–48.

McCaffrey, R., 1992. Oblique plate convergence, slip vectors, and fore-arc deformation. J. Geophys. Res. 97, 8905–8915.

McCaffrey, R., Long, M.D., Goldfinger, C., Zwick, P.C., Nabelek, J.L., Johnson, C.K., Smith, C., 2000. Rotation and plate locking at the Southern Cascadia Subduction Zone. Geophys. Res. Lett. 27, 3117–3120.

Michibayashi, K., Ohara, Y., Stern, R.J., Fryer, P., Kimura, J.-I., Tasaka, M., Harigane, Y., Ishii, T., 2009. Peridotites from a ductile shear zone within back-arc lithospheric mantle, southern Mariana Trench: results of a Shinkai 6500 dive. Geochem. Geophys. Geosyst. 10. http://dx.doi.org/10.1029/2008GC002197. Q05X06.

Ohara, Y., Reagan, M.K., Bloomer, S.H., Fryer, P., Fuji, A., Hickey-Vargas, R., Imoto, H., Ishii, T., Ishizuka, O., Johnson, J., Michibayashi, K., Ribeiro, J., Stern, R.J., Uehara, S., Satoshi, O., 2008. Structure and origin of the Mariana fore-arc and implications for the origin of continental crust: a Shinkai 6500 study of the southern Mariana fore-arc.

Ohara, Y., Reagan, M.K., Fujikura, K., Watanabe, H., Michibayashi, K., Ishii, T., Stern, R.J., Pujana, I., Martinez, F., Girard, G., Ribeiro, J., Brounce, M., Komori, N., Kino, M., 2012. A serpentinite-hosted ecosystem in the Southern Mariana Fore-arc. Proc. Natl. Acad. Sci. 109.

Pabst, S., Zack, T., Savov, I.P., Ludwig, T., Rost, D., Tonarini, S., Vicenzi, E.P., 2012. The fate of subducted oceanic slabs in the shallow mantle: insights from boron isotopes and light element composition of metasomatized blueschists from the Mariana fore-arc. Lithos 132–133, 162–179.

Parkinson, I.J., Pearce, J.A., 1998. Peridotites from the Izu–Bonin–Mariana Fore-arc (ODP Leg 125): evidence for mantle melting and melt–mantle interaction in a supra-subduction zone setting. J. Petrol. 39, 1577–1618.

Peacock, S.A., 1990. Fluid processes in subduction zones. Science 248, 329–337.

Plank, T., Cooper, L.B., Manning, C.E., 2009. Emerging geothermometers for estimating slab surface temperatures. Nat. Geosci. 2, 611–615.

Plank, T., Kelley, K.A., Zimmer, M.M., Hauri, E.H., Wallace, P.J., 2013. Why do mafic arc magmas contain ~4 wt% water on average? Earth Planet. Sci. Lett. 364, 168–179.

Plank, T., Langmuir, C.H., 1998. The chemical composition of subducting sediment and its consequences for the crust and mantle. Chem. Geol. 145, 325–394.

Reynard, B., 2013. Serpentine in active subduction zones. Lithos 178, 171–185.

Ribeiro, J.M., Stern, R.J., Kelley, K., Shaw, A., Martinez, F., Ohara, Y., 2015. Composition of the slab-derived fluids released beneath the Mariana fore-arc: evidence for shallow dehydration of the subducting plate. Earth Planet. Sci. Lett. http://dx.doi.org/10.1016/j.epsl.2015.02.018.

Roeder, P.L., Emslie, R.F., 1970. Olivine-liquid equilibrium. Contrib. Mineral. Petrol. 29, 275–289.

Savov, I.P., Ryan, J.G., D'Antonio, M., Fryer, P., 2007. Shallow slab fluid release across and along the Mariana arc-basin system: insights from geochemistry of serpentinized peridotites from the Mariana fore arc. J. Geophys. Res. 112, B09205. http://dx.doi.org/10.1029/2006JB004749.

Scambelluri, M., Tonarini, S., 2012. Boron isotope evidence for shallow fluid transfer across subduction zones by serpentinized mantle. Geology 40, 907–910.

Schmidt, M., Poli, S., 1998. Experimentally based water budgets for dehydrating slabs and consequences for magma generation. Earth Planet. Sci. Lett. 163, 361–379.

Schwartz, S., Allemand, P., Guillot, S., 2001. Numerical model of the effect of serpentinites on the exhumation of eclogitic rocks: insights from the Monviso ophiolitic massif (Western Alps). Tectonophysics 342, 193–206.

Shaw, A.M., Hauri, E.H., Fischer, T.P., Hilton, D.R., Kelley, K.A., 2008. Hydrogen isotopes in Mariana arc melt inclusions: implications for subduction dehydration and the deep-Earth water cycle. Earth Planet. Sci. Lett. 275 (1–2), 138–145.

Straub, S.M., Layne, G.D., 2002. The systematics of boron isotopes in Izu arc front volcanic rocks. Earth Planet. Sci. Lett. 198, 25–39.

Syracuse, E.M., Van Keken, P.E., Abers, G.A., 2010. The global range of subduction zone thermal models. Phys. Earth Planet. Inter. 183, 73–90.

Tatsumi, Y., 1989. Migration of fluid phase and genesis of basalt magmas in subduction zones. J. Geophys. Res., Solid Earth 94, 4697–4707.

Tonarini, S., Agostini, S., Doglioni, C., Innocenti, F., Manetti, P., 2007. Evidence for serpentinite fluid in convergent margin systems: the example of El Salvador (Central America) arc lavas. Geochem. Geophys. Geosyst. 8, Q09014.

Turner, S.J., Langmuir, C.H., 2015a. The global chemical systematics of arc front stratovolcanoes: evaluating the role of crustal processes. Earth Planet. Sci. Lett. 422, 182–193.

Turner, S.J., Langmuir, C.H., 2015b. What processes control the chemical compositions of arc front stratovolcanoes? Geochem. Geophys. Geosyst. 16, 1865–1893.

Turner, S.J., Langmuir, C.H., Katz, R.F., Dungan, M.A., Escrig, S., 2016. Parental arc magma compositions dominantly controlled by mantle-wedge thermal structure. Nat. Geosci. 9, 772–776.

Ulmer, P., Trommsdorff, V., 1995. Serpentine stability to mantle depths and subduction-related magmatism. Science 268, 858–861.

Van Keken, P.E., Hacker, B.R., Syracuse, E.M., Abers, G.A., 2011. Subduction factory: 4. Depth-dependent flux of H_2O from subducting slabs worldwide. J. Geophys. Res., Solid Earth 116, B01401. http://dx.doi.org/10.1029/2010jb007922.

Von Huene, R., Lallemand, S., 1990. Tectonic erosion along the Japan and Peru convergent margins. Geol. Soc. Am. Bull. 102, 704–720.

Wada, I., Wang, K., He, J., Hyndman, R.D., 2008. Weakening of the subduction interface and its effects on surface heat flow, slab dehydration, and mantle wedge serpentinization. J. Geophys. Res., Solid Earth 113, B04402. http://dx.doi.org/10.1029/2007jb005190.

Walowski, K.J., Wallace, P.J., Hauri, E.H., Wada, I., Clynne, M.A., 2015. Slab melting beneath the Cascade Arc driven by dehydration of altered oceanic peridotite. Nat. Geosci. 8, 404–408.

Wright, D.J., Bloomer, S.H., MacLeod, C.J., Taylor, B., Goodlife, A.M., 2000. Bathymetry of the Tonga trench and fore-arc: a map series. Mar. Geophys. Res. 21, 489–511.